

Entanglement Enhanced Sensing with Qubits affected by non-Markovian Dephasing

Noah Kaufmann,¹ Kasper Hede Nielsen,^{1,2} and Anders Søndberg Sørensen¹

¹*Center for Hybrid Quantum Networks (Hy-Q), The Niels Bohr Institute, University of Copenhagen, Jagtvej 155A, Copenhagen DK-2200, Denmark*

²*NNF Quantum Computing Programme, The Niels Bohr Institute, University of Copenhagen, Blegdamsvej 17, Copenhagen DK-2100, Denmark*

Entanglement has been proposed as a means to improve the sensitivity of sensing weak signals. While the degree of this quantum advantage is well understood in noiseless settings, the situation is more complex under realistic conditions, where the system is subject to decoherence. In this case, the enhancement depends on the specific noise characteristics. Previous treatments of colored noise typically assume that the noise is uncorrelated between successive experiments. Here, we consider the scenario in which the noise exhibits correlations across multiple shots. We derive a simple fundamental limit to the sensitivity based on the fact that the sensitivity cannot be better than the signal-to-noise ratio seen by the probe. Focusing on Ramsey spectroscopy with probes affected by pure classical dephasing, we show that, for suitable spatial and temporal noise correlations, entangled probes achieve a better scaling of the sensitivity with the number of probes than separable states. This demonstrates that entanglement can provide a substantial improvement for Ramsey spectroscopy subject to correlated noise.

I. INTRODUCTION

High-precision measurements are central to exploring new physics [1]. An improved understanding of physical processes, in particular in atomic, molecular, and optical systems, has led to the development of highly sensitive sensors [2]. Such devices enable the measurement of even minuscule effects, thereby opening a window into previously unobserved phenomena and enabling an improved understanding of nature. To further push the frontier in sensitivity, quantum entanglement has been suggested [3] and experimentally demonstrated [4, 5], as a next resource for enhancing measurement precision.

The uncertainty in estimating a parameter from N independent probes scales as $1/\sqrt{N}$, a consequence of the central limit theorem [6]. Quantum enhanced sensing aims to surpass this so-called standard quantum limit by taking advantage of entangled probes [7]. The ultimate bound imposed by quantum mechanics, called the Heisenberg limit, scales as $1/N$ [8, 9] and is achievable in noiseless settings [8, 10]. In realistic, noisy settings, however, entanglement does not necessarily enable improved scaling [11, 12], and whether the advantage persists depends on the precise noise characteristics.

A widely studied paradigm for exploring entanglement-enhanced sensing employs various types of Ramsey spectroscopy [13]. Typically, the sensors are two-level systems whose energy splitting depends on the amplitude of an external field, enabling its estimation. When these sensing qubits are prepared in a superposition of energy eigenstates and exposed to the external field, they accumulate a relative phase that depends on the field strength. By subsequently measuring that phase, one can estimate the external field strength. The estimation uncertainty arises both from the probabilistic measurement outcomes and from noise affecting the phase evolution. Given fixed resources, namely the total interrogation time T and the number of two-level systems N ,

and assuming no bias, the objective is to minimize the estimation uncertainty of the external field by optimizing the initial state preparation, the measurement procedure, and the number of shots of the experiment L that are conducted within the total time T . In particular, we are interested in the asymptotic estimation uncertainty scaling, which describes the limit for large N and T [14].

For separable resources and in the absence of noise, it is optimal to prepare each of the qubits in an even superposition of the energy eigenstates, leading to the standard quantum limit $1/\sqrt{N}$ [6]. The first proposal for entanglement-enhanced sensing in this setting involved the preparation of spin-squeezed states [15, 16]. Later work showed that, under noiseless conditions, maximally entangled GHZ states are optimal and achieve the Heisenberg scaling of $1/N$ [8]. However, when qubits are affected by independent Markovian dephasing, estimation protocols using GHZ states lose their advantage over separable strategies [11], while partially entangled states, such as spin-squeezed states, offer an improvement by a constant factor [11, 17]. Indeed, it has been proven that surpassing a scaling of $1/\sqrt{N}$ is not possible in the presence of independent Markovian dephasing [12]. For non-Markovian noise, in contrast, it was argued that an estimation uncertainty scaling of $1/N^{3/4}$ is achievable with GHZ states [18, 19] and that this scaling, known as the Zeno limit, is optimal [20]. This scaling was shown to be a general property of dephasing noise that is correlated at short times [21, 22].

These results for colored noise [18–22] were derived using the quantum Cramér–Rao bound [23], where the estimation uncertainty for L experimental shots is obtained by dividing the uncertainty of a single shot by the square root of the number of shots, \sqrt{L} . This implicitly assumes that the noise is uncorrelated across different shots of the experiment, which implies that the noise must be reset after every Ramsey sequence [20, 24, 25]. While such an assumption may be justified for some experimental sce-

narios, e.g., cold atom experiments [26], which have a limited interrogation time before the atoms are lost, it is generally incompatible with the temporal correlations inherent to non-Markovian noise. Whether entanglement can enhance quantum sensing in the setting of correlated experimental shots thus remains an open question.

The results mentioned so far consider the noise among the N sensing qubits to be uncorrelated. In the opposite case, called collective dephasing, where all N probes are subject to the same noise, the estimation uncertainty generally scales unfavorably compared to the spatially uncorrelated noise [27–29]. More recently, Ramsey spectroscopy has been studied in the presence of more general spatial noise correlations. In particular, superclassical scaling has been demonstrated for negatively correlated spatial noise with GHZ and one-axis twisted states in scenarios where the distances between probes are randomized [30] or engineered [31]. Furthermore, a fundamental uncertainty bound for parameter estimation in the presence of spatially correlated Markovian noise has been derived, revealing which spatial noise correlations allow for an entanglement advantage [32].

In this work, we extend the analysis of entanglement-enhanced quantum sensing to noise that is both temporally and spatially correlated, including correlations between experimental shots. We first derive a fundamental limit for quantum sensing, which, in short, states that the signal-to-noise ratio of a sensing experiment cannot exceed the signal-to-noise ratio experienced by the system sensing the signal. This very simple statement is shown to, e.g., capture the sensing limit identified in Ref. [11, 12]. We then demonstrate that, for non-Markovian temporal noise, entanglement can indeed substantially enhance the sensitivity of sensors with entangled probes compared to those with separable probes. In particular, for spin-squeezed states, we show that an uncertainty scaling of $1/N^{3/4}$ is achievable, provided that the environment has a suitable noise spectrum. Finally, we consider combined temporal and spatial noise correlations, showing that anti-correlated spatial noise can support enhanced scaling.

We emphasize that the present study considers quantum sensing, where the goal is to estimate an unknown external field. Although similar techniques, e.g., Ramsey spectroscopy, are often used, this is different from atomic clocks, where the aim is to stabilize a noisy local oscillator. For atomic clocks, the previous discussion therefore does not apply. Instead, it was shown in Refs. [33–35] that near Heisenberg scaling may be achieved even for Markovian noise.

II. FUNDAMENTAL LIMIT FOR FREQUENCY ESTIMATION

We consider a collection of two-level systems with internal levels $|0\rangle$ and $|1\rangle$, and energy splitting $\hbar b$ ($\hbar = 1$ in the following) induced by an external field b that we want

to determine with high precision. A prominent example is spin qubits used to detect magnetic fields via the Zeeman effect. The minimal uncertainty of the obtained estimate b_{est} of the field b depends on the number of qubits N , the total sensing time T , and the noise affecting the system. In this section, we derive a lower bound on the uncertainty in estimating a time-independent frequency b in terms of the resources N and T , assuming stationary, translationally invariant, classical, pure dephasing noise.

The system Hamiltonian H_S of an N -qubit system with energy splitting b is given by

$$H_S = \frac{b}{2} \sum_{n=1}^N \sigma_z^{(n)}, \quad (1)$$

where σ_k , with $k = x, y, z$, denote the Pauli matrices. The evolution of the system and its environment is described by the Hamiltonian $H = H_S + H_{SE} + H_E$, where H_{SE} denotes the interaction Hamiltonian with the environment, and H_E the Hamiltonian of the environment. In this work, we restrict to pure dephasing noise, $H_{SE} \propto \sigma_z$, where the system and interaction Hamiltonian commute, $[H_S, H_{SE}] = 0$. This type of ‘parallel’ noise is considered to be most harmful for frequency estimation [22], and for uncorrelated noise, limits the asymptotic scaling of the estimation uncertainty [36].

In the interaction picture with respect to H_E , we can represent the interaction Hamiltonian as

$$\tilde{H}_{SE} = \frac{1}{2} \sum_{n=1}^N \sigma_z^{(n)} \otimes [b\mathbb{I} + F_n(t)], \quad (2)$$

where $F_n(t)$ are bath operators [30]. Generally, $F_n(t)$ are operators with a non-trivial commutation relation $[F_n(0), F_m(t)] \neq 0$. In this work, we restrict ourselves to classical environments where $F_n(t)$ are real stochastic processes and hence $[F_n(0), F_m(t)] = 0$ [37, 38]. For a bosonic bath, this assumption is valid in the high-temperature regime, where the occupancy of all relevant noise modes is much larger than unity, which can be expressed as $\beta\omega_c \ll 1$, where ω_c is the highest relevant noise frequency and $\beta = 1/(k_B T)$ the inverse temperature [22, 39]. Under the classical pure dephasing assumption, the system dynamics can be described by the effective Hamiltonian $H_{\text{eff}}(t)$ [39],

$$H_{\text{eff}}(t) = H_S + \frac{1}{2} \sum_{n=1}^N F_n(t) \sigma_z^{(n)}. \quad (3)$$

We assume $F_n(t)$ to be of zero mean, stationary, and translationally invariant. Expressing $F_n(t)$ for $t \in [0, T)$ with a Fourier series in time and qubit number yields

$$H_{\text{eff}}(t) = \sum_{n=1}^N \left[\frac{b+c_{00}}{2} + \sum_{s=1}^{N-1} \sum_{m=1}^{\infty} c_{sm} e^{2\pi i \left(\frac{sn}{N} + \frac{mt}{T} \right)} \right] \sigma_z^{(n)}. \quad (4)$$

As visible in H_{eff} , the signal b and the time and spatially independent noise component c_{00} contribute to the

system dynamics in an equivalent manner. We refer to this constant part of H_{eff} as H_{00} and denote by H_{var} the part that varies across qubits or time:

$$H_{00} = \frac{1}{2} \sum_{n=1}^N (b + c_{00}) \sigma_z^{(n)}, \quad H_{\text{var}} = H_{\text{eff}} - H_{00}. \quad (5)$$

H_{00} and H_{var} are uncorrelated, since the noise is assumed to be independent of the signal, and, for stationary and translationally invariant noise, $\langle c_{00} c_{sm} \rangle = 0$ for $s \neq 0$ or $m \neq 0$. Consequently, H_{var} is a noise term that can only increase the uncertainty of the estimate b_{est} , and we can lower-bound the estimation uncertainty by considering only H_{00} . Since b and c_{00} enter H_{00} equivalently, they cannot be distinguished, and the noise described by c_{00} directly enters the estimate b_{est} . This sets a lower limit for the noise of any measurement of b . Hence, we obtain a lower bound on the variance of the estimate from the noise c_{00} noise component,

$$(\Delta b_{\text{est}})^2 \geq (\Delta c_{00})^2 = \langle c_{00}^2 \rangle. \quad (6)$$

Here, the variance of the zero-frequency noise component $\langle c_{00}^2 \rangle$ can be expressed as

$$(\Delta c_{00})^2 = \frac{1}{(NT)^2} \sum_{n=0}^N \sum_{m=0}^N \int_0^T \int_0^T \langle F_n(t) F_m(t') \rangle dt dt'. \quad (7)$$

As a particular example, we first consider uncorrelated spatial and temporal noise. Inserting its autocorrelation function $\langle F_n(t) F_m(t') \rangle = A \delta_{nm} \delta(t - t')$, corresponding to a Lindblad operator $c = \sqrt{A/2} \sigma_z$, where A denotes the dephasing strength, into Eq. (7) leads to the bound

$$\Delta b_{\text{est}} \geq \sqrt{\frac{A}{NT}}. \quad (8)$$

This corresponds to the bound identified in Refs. [11, 12].

To describe more general noise spectra, we introduce the noise spectrum by Fourier transforming the autocorrelation function of the stationary and translationally invariant noise

$$D(k, \omega) = \sum_{n=-\infty}^{\infty} \int_{-\infty}^{\infty} e^{-i(kn + \omega\tau)} \langle F_0(0) F_n(t) \rangle dt. \quad (9)$$

Assuming a finite temporal and spatial correlation length t_c and n_c respectively, and assuming $T \gg t_c$ and $N \gg n_c$, we can express the bound of Eq. (6) in terms of the zero component of the noise spectra

$$\Delta b_{\text{est}} \geq \sqrt{\frac{D(0,0)}{NT}}. \quad (10)$$

This bound is derived solely from the properties of the effective Hamiltonian and is valid for any strategy to obtain b_{est} .

From Eq. (10), we can conclude that for noise spectra with $D(0,0) \neq 0$, no sensing strategy exceeds a scaling of $1/\sqrt{N}$ in the long time limit. However, this scaling can always be reached with separable strategies, and hence entanglement does not provide any scaling advantage. For $D(0,0) = 0$, the bound of Eq. (10) is trivial and, hence, useless, but it allows scaling beyond $1/\sqrt{N}$.

III. NOISY RAMSEY SPECTROSCOPY WITH SPIN-SQUEEZED STATES

Having established a fundamental limit, we now turn to analyzing the performance of concrete protocols. There exists a wide variety of protocols for measuring a static energy splitting in an N -qubit system within a fixed total interrogation time T , particularly when entangling operations are permitted during state preparation and measurements [6]. Quantum information theoretic tools, such as quantum Fisher information, have been used to derive general bounds on the sensitivity for situations where different shots of the experiment are uncorrelated [12, 18–22, 40]. Incorporating correlations across experiments into the Fisher information is challenging due to the exponential growth in the number of possible measurement outcome sequences [24, 25]. Methods capable of handling this complexity have been developed in the context of sequential measurement metrology and studied, for example, in quantum thermometry [24, 25, 41, 42]. Here, we restrict ourselves to a specific protocol with a limited set of parameters to quantify the improvement in estimation uncertainty provided by entanglement under classical pure dephasing noise. We follow the protocol of Ref. [16], which corresponds to standard Ramsey spectroscopy [13], but with the qubits being initialized in a spin-squeezed state rather than the separable state $|0\rangle^{\otimes N}$. Furthermore, we consider the local estimation regime, where the frequency b is approximately known [22], which is the most common paradigm. To quantify the entanglement enhancement, we discuss the metrological gain

$$r = \frac{\Delta b_{\text{est}}|_{\text{sep}}}{\Delta b_{\text{est}}|_{\text{ent}}} \quad (11)$$

comparing the uncertainty of standard Ramsey spectroscopy (separable), $\Delta b_{\text{est}}|_{\text{sep}}$, with that of the entangled protocol, $\Delta b_{\text{est}}|_{\text{ent}}$. We consider the estimators to be unbiased $\langle b_{\text{est}} \rangle = b$, which implies that the estimator's variance corresponds to its mean square error ($\Delta b_{\text{est}} = \langle (b_{\text{est}} - b)^2 \rangle$).

The advantage of using spin-squeezed states becomes evident from the uncertainty expression for noiseless conventional Ramsey spectroscopy. The uncertainty depends on the initial variance ΔJ_y and the initial expectation value $\langle J_z \rangle$ according to $\Delta b_{\text{est}} \propto \Delta J_y / \langle J_z \rangle$ [15], where $J_k = 1/2 \sum_n \sigma_k^{(n)}$, with $k = x, y, z$, is the spin operator in the k -direction. For separable input states,

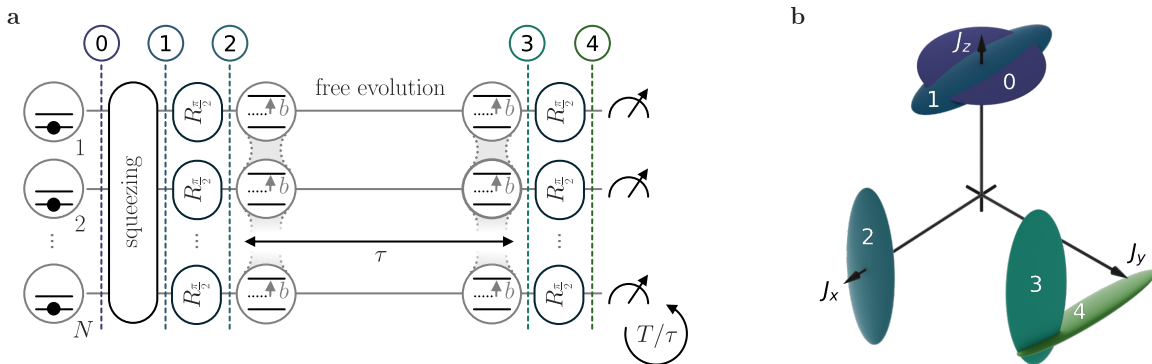


Figure 1. (a) Circuit representation of Ramsey spectroscopy using spin-squeezed states. Applying squeezing to the N -qubit ground state reduces $\langle J_y^2 \rangle$ and, to a lesser degree, $\langle J_z \rangle$. Next, a $\pi/2$ pulse ($R_{\pi/2}$) rotating the collective spin around the J_y -axis is applied. The state subsequently freely evolves for a time τ , during which it accumulates a relative phase proportional to the energy splitting. This phase is finally estimated by applying another $\pi/2$ pulse and a measurement in the J_z -basis. The total procedure is repeated T/τ times. (b) Schematic representation of the quantum state at different stages of the protocol, shown on the Bloch sphere. The ellipsoids are centered at the expectation values of the spin operators $\langle J_k \rangle$, with $k = x, y, z$, and the axis length represents their uncertainty ΔJ_k . The disc labeled with 0 depicts the unsqueezed state with $\Delta J_z = 0$ and $\Delta J_x = \Delta J_y$. The Ramsey pulses correspond to a rotation of the ellipsoids by an angle of $\pi/2$ around the J_y axis. The phase accumulation during the free evolution results in a rotation around the J_z axis. The uncertainty of the final measurement in the J_z basis is given by the width of ellipsoid 4 along the J_z direction. This illustrates how squeezing the initial state reduces shot noise and thereby improves the precision of the phase estimation.

$\Delta J_y / \langle J_z \rangle \geq 1/\sqrt{N}$ leads to a frequency estimation uncertainty scaling as $1/\sqrt{N}$, known as the shot-noise limit, since it arises from the probabilistic nature of spin measurements. Spin-squeezed states [15, 16, 43] allow $\Delta J_y / \langle J_z \rangle < 1/\sqrt{N}$ and can, assuming no other sources of noise, exceed the shot-noise limit. Moreover, spin-squeezed states are highly symmetric states with controllable entanglement. This is advantageous since, for Markovian dephasing, it was shown that symmetric states with limited entanglement outperform the more entangled GHZ states [11]. For these reasons, spin-squeezed states are a well-established resource for demonstrating quantum-enhanced Ramsey spectroscopy [11, 16, 31, 44], analogous to the use of photonic squeezed states in Mach-Zehnder interferometry [7].

The protocol considered, illustrated in Fig. 1, consists of the following steps:

1. Preparation of a spin-squeezed state;
2. $\pi/2$ pulse around the collective spin J_y -axis;
3. Free evolution of the system for a time τ ;
4. $\pi/2$ pulse around the collective spin J_y -axis;
5. Measurement of the collective spin component J_z ;
6. Repetition of steps 1-5 for $L = T/\tau$ repetitions.

This description is in the rotating frame of the field that implements the $\pi/2$ Ramsey pulses, which rotates around the J_z -axis with tunable frequency b_p . In this frame, the relative phase between the excited and ground states evolves at a frequency $b_r = b - b_p$. We assume that the duration of state preparation, measurement, and pulse operations is negligible compared to the free evolution time τ , such that the total interrogation time is effectively $T = L\tau$.

Throughout the L experiments, we consider that the state preparation and the evolution time τ are kept constant. This leaves three free experimental parameters: the amount of squeezing, the evolution time τ , and the operating point of the sensor $b_r\tau$. To parametrize the squeezing with a single parameter, κ , we consider the following class of states [44]:

$$|\psi_\kappa\rangle = \mathcal{N}(\kappa) \sum_{m=-N/2}^{N/2} (-1)^m e^{-\frac{m^2}{N\kappa^2}} |m\rangle_y, \quad (12)$$

where $\kappa \in (0, 1]$ is the squeezing parameter, $\mathcal{N}(\kappa)$ the normalization and $|m\rangle_y$ the Dicke state $|N/2, m\rangle_y$ in the y -basis. For $\kappa = 1$, up to an error in approximating the binomial distribution with a Gaussian, we recover a coherent spin state. For $\kappa < 1$ we have a spin-squeezed state with $\Delta J_y / \langle J_z \rangle < 1/\sqrt{N}$. From the state in Eq. (12), any expectation values of the spin operators can be calculated. The states are symmetric with respect to particle exchange and $\langle J_y \rangle = \langle J_x \rangle = 0$. We consider these states since they form a simple class that allows easy evaluation of all relevant expectation values. The states produced experimentally may, however, not have this form. In App. A we compare these states to those produced by the commonly considered one- and two-axis squeezing. These are found to perform similarly, except in certain situations, where the one-axis twisting may not be able to produce sufficient amounts of squeezing.

For the derivation of the uncertainty of the estimation, we operate in the Heisenberg picture and use the effective Hamiltonian of Eq. (3). The measurement operator $M_l(\tau)$ of the l -th experiment is derived by evolving the spin operators through the Ramsey sequence to the time

of measurement,

$$M_l(\tau) = \sum_{n=1}^N \left[-\cos(b_r\tau + \phi_{nl\tau}) S_z^{(ln)}(0) + \sin(b_r\tau + \phi_{nl\tau}) S_y^{(ln)}(0) \right], \quad (13)$$

where $\phi_{nl\tau} = \int_{l\tau}^{(l+1)\tau} F_n(t) dt$ and $S_k^{(ln)}(0)$ are the spin operators ($S_k = \sigma_k/2$) of qubit n before the first Ramsey pulse of experimental shot l . We assume that $\phi_{nl\tau}$ has a Gaussian distribution with zero mean. Unlike previous treatments of colored noise [18, 19], we consider the noise to be correlated between different experimental shots and qubits, meaning $\langle \phi_{nl\tau} \phi_{n'l'\tau} \rangle$ is not necessarily 0 for $l \neq l'$ or $n \neq n'$.

The response of the measurement outcome to changes in the signal $|\partial \langle M_l(\tau) \rangle / \partial b|$ is maximal for $b_r\tau = q\pi/2$, with odd q . We consider operating the sensor around this point of optimal response and denote the deviation from the optimal point by the phase θ ,

$$M_l(\tau) = \sum_{n=1}^N \left[\sin(\theta + \phi_{nl\tau}) S_z^{(ln)}(0) + \cos(\theta + \phi_{nl\tau}) S_y^{(ln)}(0) \right]. \quad (14)$$

Operating in the local estimation regime, meaning $\theta \ll 1$, we linearize the relation between b and $\langle M_l(\tau) \rangle$. With these assumptions, the frequency estimate b_{est} is obtained from the measurement outcomes m_l according to

$$b_{\text{est}} = \frac{1}{L} \sum_{l=1}^L \frac{m_l}{\frac{\partial \langle M_l(\tau) \rangle}{\partial b}} + b_p, \quad (15)$$

where b_p is the frequency of the rotating frame. To ensure that the estimator is unbiased [31], we consider the case where the noise-dependent slope $\partial \langle M_l(\tau) \rangle / \partial b$ is known from sensor calibration and assume that the experiments are affected by the same noise as during calibration.

The estimation uncertainty Δb_{est} is given by the ratio of the variance of the total measurement $M(\tau) = \sum_l M_l(\tau)$ and the response of $\langle M(\tau) \rangle$ to changes in b [45],

$$\Delta b_{\text{est}} = \frac{\Delta M(\tau)}{L \left| \frac{\partial \langle M_0(\tau) \rangle}{\partial b} \right|}, \quad (16)$$

where we used that for stationary noise $\langle M_l(\tau) \rangle$ is independent of l . To evaluate Eq. (16) with Eq. (14) we do a first-order approximation in θ ,

$$\begin{aligned} \sin(\theta + \phi_{nl\tau}) &\approx \frac{(1+i\theta)e^{i\phi_{nl\tau}} - (1-i\theta)e^{-i\phi_{nl\tau}}}{2i} \\ \cos(\theta + \phi_{nl\tau}) &\approx \frac{(1+i\theta)e^{i\phi_{nl\tau}} + (1-i\theta)e^{-i\phi_{nl\tau}}}{2}. \end{aligned} \quad (17)$$

Using that, for a Gaussian random variable X , $\langle e^{iX} \rangle = e^{-\langle X^2 \rangle / 2}$, and keeping terms up to first order in θ , we obtain

$$\begin{aligned} \langle \sin(\theta + \phi_{00\tau}) \sin(\theta + \phi_{nl\tau}) \rangle &\approx e^{-\gamma(\tau)} \sinh \langle \phi_{00\tau} \phi_{nl\tau} \rangle \\ \langle \cos(\theta + \phi_{00\tau}) \cos(\theta + \phi_{nl\tau}) \rangle &\approx e^{-\gamma(\tau)} \cosh \langle \phi_{00\tau} \phi_{nl\tau} \rangle, \end{aligned} \quad (18)$$

where the dephasing is contained in the function $\gamma(\tau) = \langle \phi_{nl\tau}^2 \rangle$. These equations, combined with the properties of the introduced spin-squeezed states $\langle J_y(0) \rangle = \langle J_x(0) \rangle = 0$ and the assumption that the spins are initialized at each shot such that the spins of different experiments are uncorrelated, lead to the estimation uncertainty

$$\begin{aligned} (\Delta b_{\text{est}})^2 &= \left\{ \frac{NL}{4} e^{\gamma(\tau)} - \frac{L}{4(N-1)} \sum_{n \neq n'}^N e^{\langle \phi_{n0\tau} \phi_{n'0\tau} \rangle} + \frac{\langle J_z(0) \rangle^2}{N^2} \sum_{n, n'}^N \sum_{l \neq l'}^L \sinh(\langle \phi_{nl\tau} \phi_{n'l'\tau} \rangle) \right. \\ &\quad \left. + \frac{L}{N(N-1)} \sum_{n \neq n'}^N \left[\langle J_z(0) \rangle^2 \sinh(\langle \phi_{n0\tau} \phi_{n'0\tau} \rangle) + \langle J_y(0) \rangle^2 \cosh(\langle \phi_{n0\tau} \phi_{n'0\tau} \rangle) \right] \right\} \left\{ T \langle J_z(0) \rangle \right\}^{-2}. \end{aligned} \quad (19)$$

This expression will form the basis of our analysis of the estimation uncertainty.

IV. UNCERTAINTY ANALYSIS

In this section, we discuss Eq. (19) for different spatial and temporal noise spectra. We start by briefly discussing the well-established scenarios of no- and uncorrelated noise. We then turn to non-Markovian temporal and spatially correlated noise with correlations between different shots of the experiment. A regime that has been disregarded so far.

A. No noise

By setting $\phi_{nl\tau} = 0$ in Eq. (19) we recover the well-known estimation uncertainty in the absence of noise [15],

$$\Delta b_{\text{est}} = \frac{\Delta J_y(0)}{\sqrt{T\tau} \langle J_z(0) \rangle}. \quad (20)$$

The presence of uncertainty in estimating b , even in the absence of external noise, arises from the probabilistic nature of measurements. For separable input states, the ratio $\Delta J_y / \langle J_z \rangle$ is lower bounded by $1/\sqrt{N}$, leading to a scaling of $\Delta b_{\text{est}} = 1/\sqrt{\tau TN}$, known as the shot noise

limit [46], while for spin-squeezed states this ratio is lowered and can reach the lower bound $1/N$ [47]. Consequently, spin squeezing improves the uncertainty scaling in the absence of noise [15].

B. Uncorrelated noise

Temporally uncorrelated noise, called white or Markovian, which is also spatially uncorrelated, is characterized by $\langle \phi_{nk\tau} \phi_{n'k'\tau} \rangle = A\tau \delta_{nn'} \delta_{kk'}$ and consequently $\gamma(\tau) = A\tau$. Under these noise properties, Eq. (19) simplifies to

$$(\Delta b_{\text{est}})^2 = \frac{\frac{N}{4} (e^{A\tau} - 1) + \langle J_y(0)^2 \rangle}{T\tau \langle J_z(0) \rangle^2}. \quad (21)$$

For separable input states, with $\langle J_z(0) \rangle = N/2$ and $\langle J_y(0)^2 \rangle = N/4$, the optimal interrogation time is given by $\tau = 1/A$, leading to an estimation uncertainty of $\Delta b_{\text{est}}|_{\text{sep}} = \sqrt{Ae}/\sqrt{NT}$. This sets the minimal achievable uncertainty for all separable strategies [11]. By introducing spin-squeezed input states, the optimization involves both the squeezing parameter κ and the interrogation time τ . While entanglement does not alter the $1/\sqrt{T}$ scaling, increasing N enhances the metrological gain r defined in Eq. (11), as illustrated in Fig. 2. However, r cannot exceed \sqrt{e} due to the fundamental limit of Eq. (6), and hence, in the case of Markovian dephasing noise, entanglement only offers a constant-factor enhancement over separable strategies [12]. Notably, $r = \sqrt{e}$ cannot be reached with maximally entangled GHZ states, but it can be approached using spin-squeezed states, which are highly symmetric yet only partially entangled [11, 17].

C. Temporally correlated and spatially uncorrelated noise

In this subsection, we discuss general temporally correlated but spatially uncorrelated noise, i.e.,

$$\langle \phi_{nl\tau} \phi_{n'l'\tau} \rangle = \delta_{nn'} Q_\tau(l - l'). \quad (22)$$

Given a temporal noise spectra $S(\omega)$ we can evaluate $Q_\tau(\Delta_l)$ to be [48, 49]

$$Q_\tau(\Delta_l) = \frac{\tau^2}{\pi} \int_0^\infty S(\omega) \text{sinc}\left(\frac{\tau\omega}{2}\right)^2 \cos(\tau\omega\Delta_l) d\omega, \quad (23)$$

where the sinc-function emerges from the Fourier transform of the rectangular time window of a single Ramsey sequence and $\Delta_l = l - l'$.

In addition to the Markovian noise spectrum $S_W(\omega)$, we consider three non-Markovian noise spectra, each

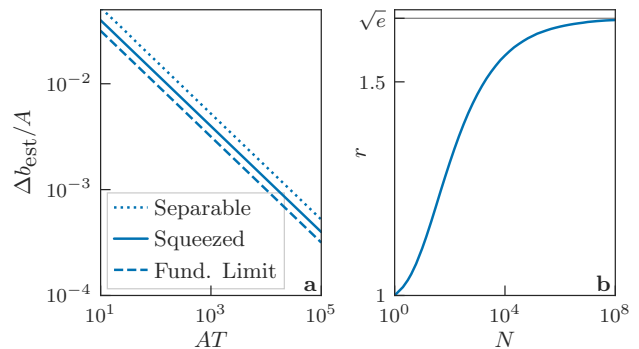


Figure 2. Comparison of estimation uncertainty in Ramsey spectroscopy using separable and spin-squeezed input states in the presence of spatially and temporally uncorrelated noise characterized by a strength A . (a) The estimation uncertainty $\Delta b_{\text{est}}/A$ as a function of the total time AT for a fixed number of qubits $N = 100$. The dotted line indicates unsqueezed states, the full line corresponds to squeezed states, and the dashed line indicates the fundamental limit. All curves scale with $1/\sqrt{T}$ and differ only by constant factors. (b) The metrological gain r between the uncertainties of the spin-squeezed and separable protocols at fixed $AT = 1000$ as a function of N . As N increases, the uncertainty of the spin-squeezed protocol approaches the fundamental limit of Eq. (6), yielding an asymptotic improvement by a factor of \sqrt{e} compared to the separable protocol.

characterized by a noise strength A and a characteristic frequency σ :

$$\begin{aligned} S_W(\omega) &= A, \\ S_G(\omega) &= Ae^{-\frac{\omega^2}{2\sigma^2}}, \\ S_L(\omega) &= A \left(1 - e^{-\frac{|\omega|}{\sigma}}\right), \\ S_O(\omega) &= A \frac{|\omega|}{\sigma} e^{-\frac{|\omega|}{\sigma}}. \end{aligned} \quad (24)$$

The noise with a Gaussian spectrum $S_G(\omega)$ represents correlated noise with a correlation time $1/\sigma$, as its autocorrelation function is also Gaussian. The linear spectrum $S_L(\omega)$, which is linear at small frequencies and flat at high frequencies, is an example of temporally anti-correlated noise. Its autocorrelation function consists of a delta peak at $t = 0$ and a negative Lorentzian with a time scale $1/\sigma$. Finally, the Ohmic spectrum $S_O(\omega)$ corresponds to noise that is correlated at short times and anti-correlated at longer times. An example of the spectra is illustrated in Fig. 3a. The autocorrelation function and the dephasing $\langle \phi_{00\tau}^2 \rangle = \gamma(\tau)$ for the noise spectra of Eq. (24) are given in App. B.

Simplifying Eq. (19) for spatially uncorrelated noise

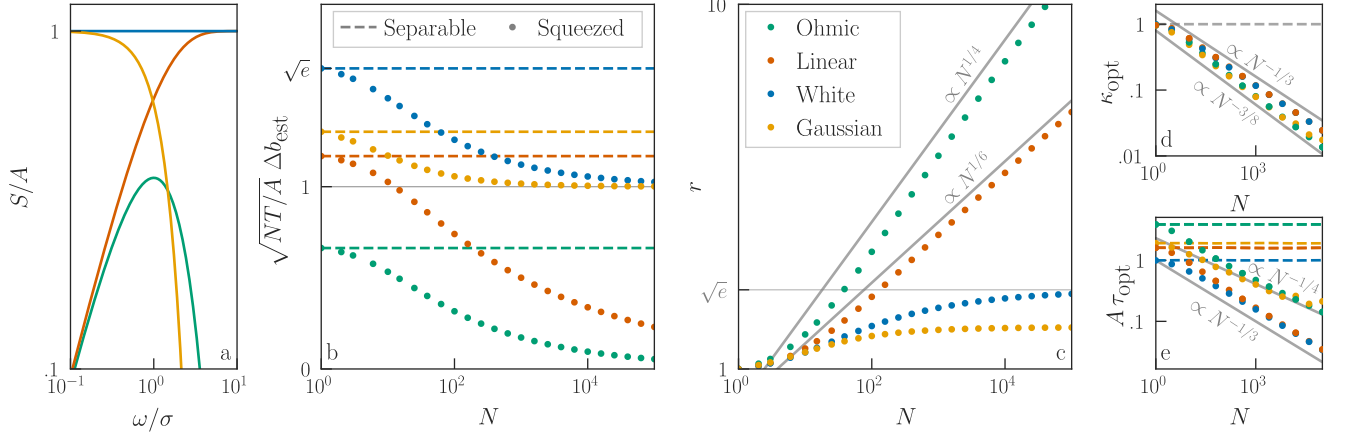


Figure 3. Estimation uncertainty of Ramsey spectroscopy with separable and spin-squeezed input states for different noise spectra and a certain total probing time T much larger than the noise correlation time and dephasing time. (a) The considered noise spectra. We choose $\sigma/A = 1/2$. (b) The uncertainty scaled with $\sqrt{NT/A}$ as a function of the number of qubits N for spin-squeezed and separable input states under noise with (counting from below at $N = 1$) Ohmic, linear, Gaussian, and white spectra. For the Gaussian and white noise, the uncertainty approaches the fundamental limit of Eq. (6), which is $\Delta b_{\text{est}} = \sqrt{A/NT}$. For the linear and Ohmic noise, on the other hand, the noise is zero at zero frequency, meaning that Eq. (6) does not pose a constraint. We therefore find a large improvement from using spin-squeezed states. (c) The metrological gain r , corresponding to the ratio of the estimation uncertainty with and without squeezing. The optimal interrogation time τ and squeezing parameter κ are displayed in (d) and (e).

leads to

$$(\Delta b_{\text{est}})^2 = \frac{\langle J_y(0)^2 \rangle}{\tau T \langle J_z(0) \rangle^2} + \frac{N [e^{\gamma(\tau)} - 1]}{4\tau T \langle J_z(0) \rangle^2} + \frac{\sum_{l \neq l'}^L \sinh[\langle \phi_{0l\tau} \phi_{0l'\tau} \rangle]}{NT^2}. \quad (25)$$

The last term in Eq. (25) accounts for correlations among experimental shots. Leaving this term out corresponds to the scenario in which the noise is reset after each Ramsey sequence, as discussed in Refs. [18–20].

For a discussion of Eq. (25), but not for the displayed numerical results, we expand $\sinh x = x + O(x^3)$ and drop the higher order terms, assuming $\langle \phi_{0k\tau} \phi_{0k'\tau} \rangle$ to be small, which leads to

$$(\Delta b_{\text{est}})^2 \approx \frac{\langle J_y(0)^2 \rangle}{\tau T \langle J_z(0) \rangle^2} + \frac{N [e^{\gamma(\tau)} - 1]}{4\tau T \langle J_z(0) \rangle^2} - \frac{\gamma(\tau)}{N\tau T} + \frac{\gamma(T)}{NT^2}. \quad (26)$$

The last term of Eq. (26) is independent of the precise quantum state of the system and the interrogation time τ . In the long-time limit, Δb_{est} scales with $1/\sqrt{T}$ and $\gamma(T)/T$ can be approximated by the zero-frequency noise component $S(0)$ (see App. C). As the sum of the first three terms in Eq. (26) is positive, we immediately recover the fundamental bound of Eq. (6) from the last term.

Unlike the last term, the sum of the first three terms on the right-hand side of Eq. (26) depends on the squeezing parameter κ and the interrogation time τ . We consider

the long-time limit such that the optimal duration of a single experiment τ_{opt} satisfies $\tau_{\text{opt}} \ll T$, i.e., where we perform many Ramsey sequences. Decreasing κ , which corresponds to introducing more entanglement, reduces the first term associated with the shot noise as described in Eq. (20). However, additional squeezing also suppresses $\langle J_z(0) \rangle$ and thus increases the second term. The interrogation time τ introduces a different tradeoff. Reducing τ increases the shot-noise term but decreases the sum of the second and third terms, which are linked to dephasing. The interplay between these effects determines the ideal parameters. The optimal values of κ and τ depend mainly on the short-time behavior of $\gamma(\tau)$, which determines how the second and third terms scale with τ . Finally, a larger number of qubits N enables stronger squeezing and a shorter optimal interrogation time, leading to a lower estimation uncertainty.

In Fig. 3b, we show the minimal uncertainty of Eq. (25), obtained by numerically optimizing both the squeezing and the interrogation time for the four noise spectra defined by Eq. (24). We rescale the obtained result such that for separable states, we get flat lines. Introducing entanglement through squeezing improves the uncertainty for higher N compared to the separable case. As visible in Fig. 3d, the optimal interrogation time decreases with increasing N . Simultaneously, the squeezing parameter κ also decreases, as shown in Fig. 3e, corresponding to stronger entanglement. For the noise spectra with a nonzero zero-frequency noise component, i.e., Gaussian and white spectra, Eq. (6) limits the normalized uncertainty to be greater than 1 in the rescaled param-

eters. In contrast, for the linear and Ohmic spectra, no such limit exists, allowing for a substantial improvement of the estimation uncertainty. This behavior is also visible in Fig. 3c, where the gain r saturates with increasing N for white and Gaussian noise, while it remains N dependent for Ohmic and linear noise.

To quantify the observed entanglement-enhancement, we consider a generic time dependence $\gamma(\tau) \propto \tau^\nu$. Using the approximate uncertainty of Eq. (26) we can find the optimal τ and κ by solving $\partial_\tau \Delta b_{\text{est}} = 0$ and $\partial_\kappa \Delta b_{\text{est}} = 0$. In leading order, we find $\tau_{\text{opt}} \propto N^{-1/3}$ and $\kappa_{\text{opt}} \propto N^{-1/3}$ for $\nu = 1$, and $\tau_{\text{opt}} \propto N^{-1/4}$ and $\kappa_{\text{opt}} \propto N^{-3/8}$ for $\nu = 2$. For spectra with $S(0) = 0$ this leads to an uncertainty scaling as $\Delta b_{\text{est}} \propto N^{-2/3}$ for $\nu = 1$ ($r \propto N^{1/6}$), and $\Delta b_{\text{est}} \propto N^{-3/4}$ for $\nu = 2$ ($r \propto N^{1/4}$). These findings, summarized in Tab. I, agree with the observed scaling of r , τ_{opt} , and κ_{opt} in Fig. 3c-e. There we see that among the noise spectra where the uncertainty is not bound by the fundamental limit of Eq. (6), a better scaling is achievable for Ohmic noise, $r \propto N^{1/4}$, than for linear noise, $r \propto N^{1/6}$. This scaling difference can be attributed to the different short-time noise behavior, for the Ohmic spectrum $\gamma(\tau) \propto \tau^2$, while for the linear spectrum $\gamma(\tau) \propto \tau$. Hence, lowering the interrogation time in the case of Ohmic noise decreases the dephasing within a single shot more than for the linear noise. Through the above-described tradeoff between κ and $\gamma(\tau)$, this leads to a better uncertainty scaling for Ohmic noise spectra.

	$\gamma(\tau)$	$\gamma(T)$	Δb_{est}	τ_{opt}	κ_{opt}
White	$\propto \tau$	$\propto T$	$\propto N^{-1/2}$	$\propto N^{-1/3}$	$\propto N^{-1/3}$
Gaussian	$\propto \tau^2$	$\propto T$	$\propto N^{-1/2}$	$\propto N^{-1/4}$	$\propto N^{-3/8}$
Linear	$\propto \tau$	$\propto \log(T)$	$\propto N^{-2/3}$	$\propto N^{-1/3}$	$\propto N^{-1/3}$
Ohmic	$\propto \tau^2$	$\propto \log(T)$	$\propto N^{-3/4}$	$\propto N^{-1/4}$	$\propto N^{-3/8}$

Table I. Leading order scaling of short-time $\gamma(\tau)$ and long-time dephasing, $\gamma(T)$, estimation uncertainty Δb_{est} , optimal interrogation time τ_{opt} , and optimal squeezing κ_{opt} with time, respectively number of qubits N across different noise spectra.

To summarize this analysis, the noise spectrum affects the estimation uncertainty in two ways. First, the zero-frequency component of the spectrum sets a limit on the achievable uncertainty and thus determines whether an uncertainty scaling of $1/\sqrt{N}$ can be surpassed. Second, for noise spectra with $S(0) = 0$, the short-time behavior of $\gamma(\tau)$, which reflects the high-frequency characteristics of the spectrum, governs the extent to which spin squeezing can enhance the scaling of the estimation uncertainty with entangled states. Overall, entanglement improves the measurement uncertainty in all the cases considered. In the large- N limit, the smallest improvement occurs for correlated noise with $S(0) \neq 0$, while the largest improvement occurs for noise with $S(0) = 0$, with $\gamma(\tau) \propto \tau^2$.

Compared to the noise model and protocol proposed in Refs. [18, 19], where the noise among different Ramsey

sequences is considered to be uncorrelated, we observe two key differences. First, the scaling advantage reported for the Gaussian spectra [19] is absent in our case, and likewise would be absent for a Lorentzian spectrum [18], because of the non-zero zero-frequency component of the noise spectrum. Second, unlike in Refs. [18, 19], our reported scaling advantage does not depend on the super-linear scaling of $\gamma(\tau)$ in τ because we use spin-squeezed states instead of GHZ states (see App. D). However, we also report the biggest scaling advantage in the cases when the noise is correlated at short times and hence $\gamma(\tau) \propto \tau^2$.

D. Temporally and spatially correlated noise

Finally, we discuss general spatial and temporal noise, where we assume that the spatial and temporal correlations can be separated,

$$\langle \phi_{nl} \tau \phi_{n'l'\tau} \rangle = Q_\tau(l-l')P(n-n'). \quad (27)$$

In particular we define $\gamma(\tau) = Q_\tau(0)P(0)$. In the temporal case, $Q_\tau(l-l')$ describes the correlation of the temporally integrated noise. Spatially, however, we assume the probes to have no spatial extension. Hence, $P(n-n')$ represents the correlation between discrete points. We consider the probes to be aligned in a line with fixed spacing Δ_x . The Nyquist frequency in this setting is given by half the spatial sampling rate, π/Δ_x . Accordingly, we define the spatial noise via its power spectrum $G(k)$, with $k \in [-\pi/\Delta_x, \pi/\Delta_x]$. By the Wiener-Khinchin theorem [50], the spatial correlation function $P(n-n')$, which represents the spatial part of the correlation function $\langle F_n(0)F_{n'}(0) \rangle$, is the inverse Fourier transform of the power spectrum. For simplicity, we choose $\Delta_x = 1$, leading to:

$$P(n-n') = \frac{1}{2\pi} \int_{-\pi}^{\pi} G(k) e^{ik(n-n')} dk. \quad (28)$$

We discuss the same noise spectra as for temporal noise in the previous section [see Eq. (24)], but restricted to the range $k \in [-\pi, \pi]$. The estimation uncertainty in this scenario is described by Eq. (19). To analyze the expression, we expand $\sinh x$ and $\cosh x$ to lowest order in x , neglect terms of order $1/N^2$, take the long time limit, and assume the spatial noise correlation length to be much shorter than the number of particles. This leads to

$$\begin{aligned} (\Delta b_{\text{est}})^2 \approx & \frac{\langle J_y^2(0) \rangle}{\tau T \langle J_z(0) \rangle^2} + \frac{N [e^{\gamma(\tau)} - 1]}{4\tau T \langle J_z(0) \rangle^2} - \frac{\gamma(\tau)}{N\tau T} \\ & + \frac{\gamma(\tau)}{N\tau T} \frac{[\Delta J_z(0)]^2}{\langle J_z(0) \rangle^2} \left[\frac{G(0)}{P(0)} - 1 \right] + \frac{S(0)G(0)}{NT}. \end{aligned} \quad (29)$$

Comparing this equation with the simplified expression for spatially uncorrelated noise, we recover Eq. (26) by

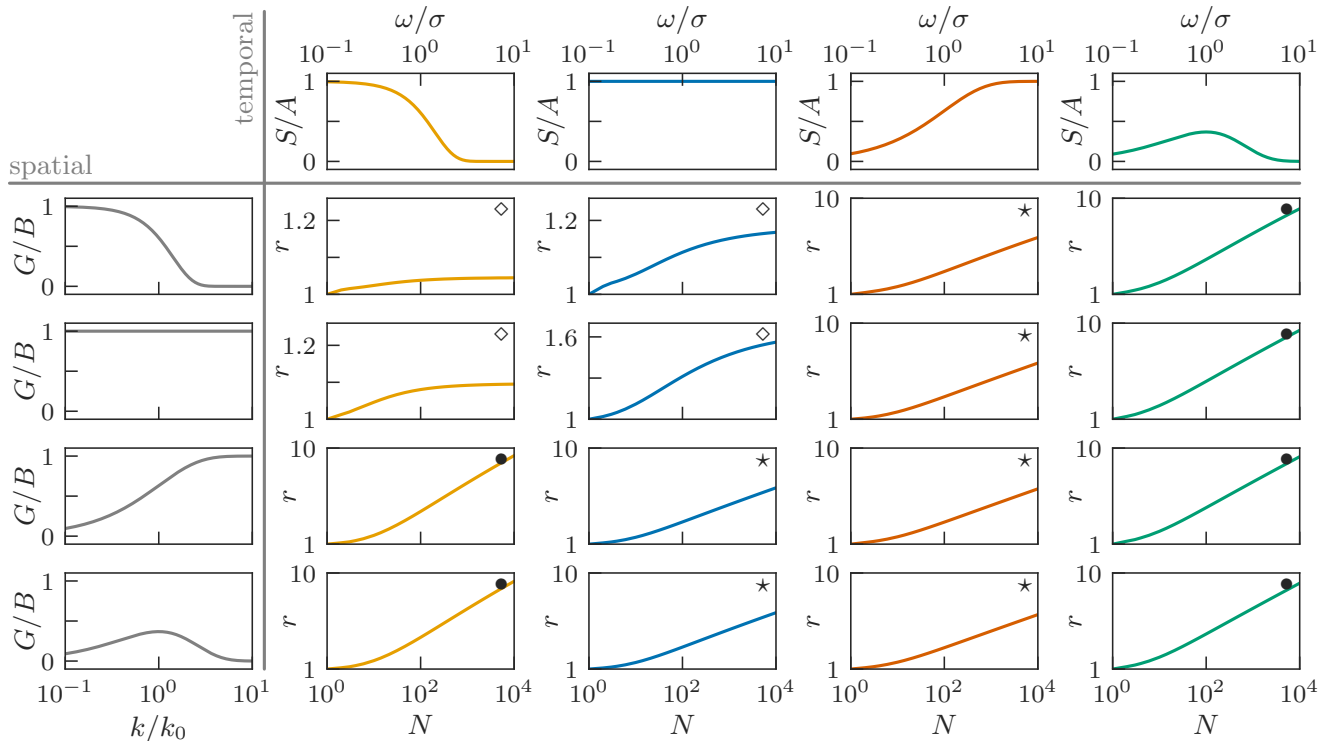


Figure 4. The metrological gain r of estimation uncertainties for separable and spin-squeezed protocols for different spatial and temporal noise correlations. The first row and first column of the grid show the considered temporal $S(\omega)$ and spatial noise $G(k)$ spectra, respectively, which are combined in the inner plots. From top to bottom and left to right, the spectra are the following: Gaussian, white, linear, and Ohmic. The temporal (spatial) spectra are characterized by strength A (B) and width σ (k_0), with $A/\sigma = 1/8$ ($B/k_0 = 1/8$). Each inner plot displays r as a function of the number of qubits N on a log-log scale, except for (\diamond) where the y-axis is scaled linearly. Symbols indicate the scaling behavior of r : (\diamond) marks cases where the estimation uncertainty only surpasses the standard quantum limit by a constant factor, (\bullet) corresponds to $r \propto N^{1/4}$, and (\star) to $r \propto N^{1/6}$.

setting $G(0) = P(0) = 1$, and we see that the first three terms remain unchanged. The last term, resembling the fundamental limit of Eq. (10), is decisive for whether a scaling beyond $\Delta b_{\text{est}} \propto 1/\sqrt{N}$ is achievable. While in the case of spatial white noise, an improved scaling required $S(0) = 0$, in the presence of spatial noise correlations, either $S(0) = 0$ or $G(0) = 0$ is sufficient. The fourth term of Eq. (29) grows with increasing squeezing, as $\Delta J_z(0)$ is zero for separable states and increases with decreasing κ . Its sign depends on whether the spatial noise is correlated or anti-correlated, $[G(0)/P(0) - 1] \geq -1$. To leading order, the fourth term scales with κ and τ the same way as the sum of the second and third terms, where the sum of the three terms is positive. Moreover, the scaling in τ of $\gamma(\tau)$ is not influenced by the spatial noise spectrum. As a result, minimizing Eq. (29) to leading order results in the same N scaling of the optimal parameters τ_{opt} and κ_{opt} as reported in Tab. I for spatially uncorrelated noise.

Fig. 4 shows the dependency of the gain r on the number of qubits N for different combinations of spatial and temporal noise. We see that for the cases where neither $G(0) = 0$ nor $S(0) = 0$, i.e., the four combinations of

Gaussian and white spectra, squeezing improves the uncertainty only up to a constant factor compared to the separable case. In these cases, we find that the advantage of using squeezing decreases with stronger noise correlations. Hence, the weakest entanglement enhancement of the measurement uncertainty is observed for noise with both temporal and spatial Gaussian correlations. Among the noise spectra in Fig. 4 with $S(0) = 0$ or $G(0) = 0$, we observe the best scaling of the metrological gain r for Gaussian and Ohmic temporal noise. In both cases, we have $\gamma(\tau) \propto \tau^2$, resulting in $r \propto N^{1/4}$. For linear and white temporal noise, $\gamma(\tau)$ only decreases linearly in τ with shorter interrogation times, leading to $r \propto N^{1/6}$.

These results illustrate that temporal and spatial noise correlations are not metrologically identical. They play a similar role in the question of whether a scaling above the standard quantum limit is possible. However, the exact scaling is determined by the shape of the temporal spectrum.

V. CONCLUSION

In this work, we have demonstrated that quantum entanglement can provide a considerable gain in the sensitivity of quantum sensing compared to Ramsey spectroscopy with separable states. Crucially, our analysis extends previous work [18, 19] by including correlations between successive experimental shots, which arise in many practical scenarios where the preparation of the system between shots does not reset the noise. Our analysis shows that an uncertainty scaling beyond the standard quantum limit of $1/\sqrt{N}$ can be achieved for classical pure dephasing noise if the zero-frequency component of the noise spectrum is zero. Intuitively speaking, this noise component at zero frequency is indistinguishable from the signal itself and therefore provides a lower limit to the uncertainty set by the signal-to-noise ratio of the signal observed by the sensors. For noise with a vanishing zero-frequency component, the optimal scaling using spin-squeezed states depends on the short-time behavior of the dephasing $\gamma(\tau)$. In the case of $\gamma(\tau) \propto \tau$, where there is no advantage to expect from GHZ states over separable states, the use of spin-squeezed states enables an uncertainty scaling as $\Delta b_{\text{est}} \propto N^{-2/3}$. For $\gamma(\tau) \propto \tau^2$, we reach an optimal scaling of $\Delta b_{\text{est}} \propto N^{-3/4}$, which corresponds to the scaling reported for GHZ states in Refs. [18, 19]. However, these works considered noise that was uncorrelated between shots of the experiments and are hence not directly comparable. While this scaling is proven to be optimal in the case of no correlations among different Ramsey sequences [20], its optimality in the presence of correlated experimental shots remains an open question. Furthermore, we emphasize that we only consider a particular sensing strategy based on standard Ramsey spectroscopy. For the considered noise sources, it may be possible to devise more optimal strategies both with and without entanglement.

ACKNOWLEDGMENTS

The authors thank Klaus Mølmer, Susana Huelga, and Martin Plenio for helpful comments. This work was supported by the Novo Nordisk Foundation (Challenge project ‘‘Solid-Q’’) and Danmarks Grundforskningsfond (Grant No. DNR139, Hy-Q Center for Hybrid Quantum Networks).

Appendix A: Spin-squeezed states

In this appendix, we extend the discussion on squeezing enhanced sensitivity of Ramsey spectroscopy to other classes of spin-squeezed states, particularly those considered more practical. So far, we focused on the spin-squeezed states $|\psi_\kappa\rangle$ defined in Eq. (12). The motivation for this choice is that their spin expectation values can be obtained easily, and varying κ allows one to continuously tune the entanglement from an approximately coherent state at $\kappa = 1$ to a maximally squeezed

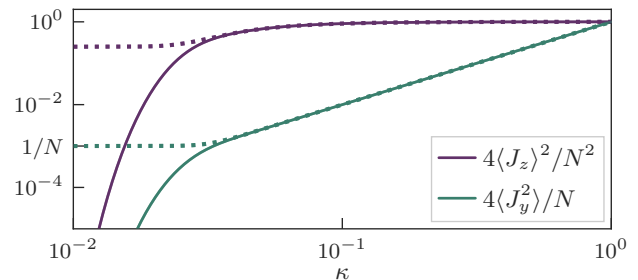


Figure 5. Dependence of the expectation values most relevant to the estimation uncertainty on the squeezing parameter κ for $N = 1000$ (solid lines) and $N = 1001$ (dashed lines) qubits. The different behavior as $\kappa \rightarrow 0$ occurs because states with an even number of qubits approach $|\psi_{\kappa \rightarrow 0}\rangle = |0\rangle_y$, while states with an odd number of qubits converge to $|\psi_{\kappa \rightarrow 0}\rangle \propto |1/2\rangle_y - |-1/2\rangle_y$.

state with $\Delta J_y / \langle J_z \rangle \propto 1/N$ for $\kappa \rightarrow 0$, as illustrated in Fig. 5. Other prominent classes of spin-squeezed states are one-axis twisted (OAT) and two-axis twisted (TAT) states [43]. From a practical perspective, these states are relevant, as they can be prepared by evolving a coherent spin state with the nonlinear Hamiltonians

$$H_{\text{OAT}} = \chi J_z^2, \quad H_{\text{TAT}} = \frac{\chi}{2i} (J_+^2 - J_-^2), \quad (\text{A1})$$

where J_\pm are the collective spin ladder operators and χ is a constant [43]. OATs have been realized experimentally in several hardware platforms through collective nonlinear interactions [45]. Recently, two-axis twisting has been demonstrated with rubidium atoms [51].

Fig. 6 compares the metrological gain of the three states over standard Ramsey spectroscopy with separable input states for uncorrelated noise and in the absence of noise. The figure is obtained by evaluating Eq. (20) and Eq. (21), for even values of N and optimizing the interrogation time and squeezing, where $\langle J_z \rangle$ and ΔJ_y are analytically evaluated for OATs [47], and numerically evaluated for $|\psi_\kappa\rangle$ and TATs. In the noise-free case, Fig. 6a, the metrological gain is proportional to $\langle J_z \rangle / (\sqrt{N} \Delta J_y)$ [see Eq. (20)]. In the limit of large N , $\Delta J_y / \langle J_z \rangle \propto 1/N$ for TATs and $|\psi_\kappa\rangle$, leading to $r \propto \sqrt{N}$ [43]. OATs reach $\Delta J_y / \langle J_z \rangle \propto N^{-5/6}$, resulting in $r \propto \sqrt[3]{N}$ [43]. For white noise, Fig. 6b, the relative ordering of the three states in terms of metrological gain remains the same. As discussed in Sec. IV B and displayed in Fig. 2b, the metrological gain is upper-bounded by \sqrt{e} . The observed differences are much smaller than in the noise-free case. We verified that all three classes of squeezed states exhibit similar behavior under the colored noise considered in Fig. 3, although OATs do not achieve the same metrological advantage as the other two classes of states for Ohmic noise, since OAT is not able to produce sufficient amounts of squeezing.

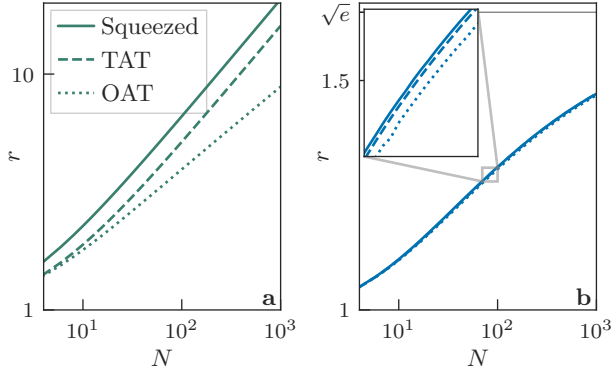


Figure 6. Comparison of the metrological gain r in Ramsey spectroscopy between spin-squeezed states $|\psi_\kappa\rangle$, defined in Eq. (12), one-axis twisted states (OAT), and two-axis twisted states (TAT), as a function of the number of probes N . The metrological gain is calculated relative to standard Ramsey spectroscopy with separable input states and is shown for the cases of (a) no noise and (b) white noise.

Appendix B: Noise properties

In this appendix, we provide the exact expressions for the dephasing behavior of the temporal noise spectra used in Sec. IV. Tab. I shows the short- and long-time limits of these expressions to the leading order. Additionally, we present the autocorrelation functions of these spectra to illustrate their temporal correlations and anti-correlations.

The analysis of the simplified uncertainty expressions of Eq. (26) and Eq. (29) shows the influence of the dephasing $\gamma(\tau) = \langle \phi_{nl\tau^2} \rangle$ on the uncertainty scaling. To evaluate $\gamma(\tau)$, we set $\Delta_l = 0$ in Eq. (23) and use the noise spectra defined in Eq. (24). This results in the following dephasing behavior:

$$\begin{aligned} \gamma_W(\tau) &= A\tau \\ \gamma_G(\tau) &= A\tau \left[\frac{1}{\tau\sigma} \sqrt{\frac{2}{\pi}} \left(e^{-\frac{\sigma^2\tau^2}{2}} - 1 \right) + \operatorname{erf} \left(\frac{\tau\sigma}{\sqrt{2}} \right) \right] \\ \gamma_L(\tau) &= A\tau \left[1 - \frac{2}{\pi} \arctan(\sigma\tau) + \frac{1}{\pi\sigma\tau} \log(1 + \sigma^2\tau^2) \right] \\ \gamma_O(\tau) &= A\tau \left[\frac{1}{\pi\sigma\tau} \log(1 + \sigma^2\tau^2) \right], \end{aligned} \quad (\text{B1})$$

where the subscripts W , G , L , and O refer to the white, Gaussian, linear, and Ohmic noise spectra as defined in Eq. (24). These functions are plotted in Fig. 7b. Their short- and long-time behavior, summarized in Tab. I, is obtained by approximating the involved functions in the regimes $\sigma\tau \ll 1$ and $\sigma\tau \gg 1$.

According to the Wiener-Khinchin theorem, the noise spectra $S(\omega)$ and the autocorrelation function $R(t)$ are related by a Fourier transform [50]. Using the non-

unitary Fourier convention, this relation reads:

$$R(t) = \frac{1}{2\pi} \int_{-\infty}^{\infty} S(\omega) e^{i\omega\tau} d\omega. \quad (\text{B2})$$

Evaluating this relation for the noise spectra in Eq. (24) gives the corresponding autocorrelation functions:

$$\begin{aligned} R_W(t) &= A\delta(t) \\ R_G(t) &= \frac{A\sigma}{2\pi} e^{-\frac{\sigma^2 t^2}{2}} \\ R_L(t) &= A \left[\delta(t) - \frac{\sigma}{\pi} \frac{1}{1 + \sigma^2 t^2} \right] \\ R_O(t) &= \frac{A\sigma}{\pi} \frac{1 - \sigma^2 t^2}{(1 + \sigma^2 t^2)^2}, \end{aligned} \quad (\text{B3})$$

where the subscripts W , G , L , and O refer to white, Gaussian, linear, and Ohmic noise spectra as defined in Eq. (24). In particular, we see that Ohmic noise is correlated for $t\sigma < 1$ and anti-correlated for $t\sigma > 1$.

Appendix C: Time dependence

In this appendix, we formalize the notion of taking the long-time limit. Furthermore, we briefly discuss the short-time behavior in the case of a single qubit for all of the considered noise spectra.

In the uncertainty analysis of Sec. IV, we considered the long-time limit of Eq. (19). This is reached when the third term on the right-hand side of Eq. (19) becomes proportional to $L = T/\tau$, such that all terms in the numerator scale linearly in T . Combined with the T^2 in the denominator, this leads to an overall scaling as $1/T$. To achieve this, we require that

$$\sum_{l \neq l'}^L \sinh(\langle \phi_{nl\tau} \phi_{n'l'\tau} \rangle) \propto L, \quad (\text{C1})$$

which holds when T is much longer than the correlation time of the noise. In this regime, we can use the relation

$$\lim_{T \rightarrow \infty} \frac{\gamma(T)}{T} = S(0), \quad (\text{C2})$$

to simplify Eq. (26) and recover the fundamental limit of Eq. (6).

For shorter times T , the situation is more complex. Fig. 7 shows the dependence of the estimation uncertainty Δb_{est} on the total time T for Ramsey spectroscopy with a single particle. In the case of white noise, the noise is not correlated between the experiments, and the uncertainty scales as $1/\sqrt{T}$ for all T . For linear noise, anti-correlations accumulate, visible in Fig. 7c at $\sigma\tau \approx 1$. For $T\sigma \ll 1$, $\gamma(T)/T \propto 1$, while for $T\sigma \gg 1$, $\gamma(T)/T \propto \log(T)/T$. Although this does not affect the overall scaling, it reduces the prefactor around $T\sigma \approx 1$.

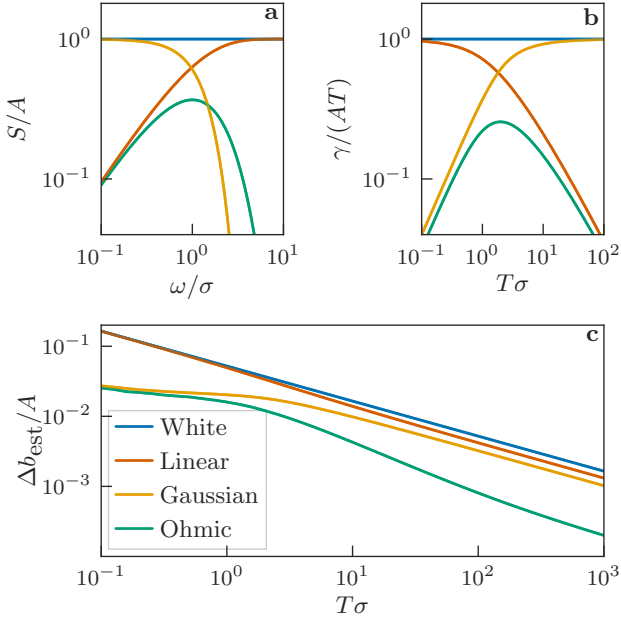


Figure 7. Estimation uncertainty of Ramsey spectroscopy with a single particle as a function of the total time T for different noise spectra. (a) Plot of the considered white, Gaussian, linear, and Ohmic noise spectra $S(\omega)$, with $\sigma/A = 1/10^3$. (b) Normalized dephasing rate $\gamma(T)/T$ as a function of the total time T . For white noise $\gamma(T) \propto T$, Gaussian noise with temporal correlations leads to $\gamma(T) \propto T^2$, the anti-correlations of linear noise result in noise cancellations, and for Ohmic noise, the noise is first correlated and for longer times anti-correlated, resulting in noise $\gamma(t)$ peaking around $\sigma T = 1$. (c) Corresponding single qubit estimation uncertainty Δb_{est} as a function of T .

When the noise spectrum is Gaussian, for $T\sigma \ll 1$ all experiments are exposed to strongly correlated dephasing $\langle \phi_{nl\tau} \phi_{n'l'\tau} \rangle \approx \delta_{n,n'} \gamma(\tau)$. In this regime, additional repetitions do not average out the noise, giving $\gamma(T)/T \propto T$, resulting in almost no improvement in the uncertainty with increasing T . For $T\sigma \gg 1$, most of the experiments are uncorrelated, so that $\gamma(T)/T \propto 1$, and the standard $1/\sqrt{T}$ scaling is recovered. For noise with an Ohmic spectrum, noise correlations, similar to the Gaussian case, for $T\sigma \ll 1$ are combined with the properties of linear noise in the regime $T\sigma \gg 1$. This leads to a scaling almost independent of T for $T\sigma \ll 1$ and a scaling $1/\sqrt{T}$ for $T\sigma \gg 1$.

Appendix D: GHZ states

In the discussion of entanglement-enhanced Ramsey spectroscopy, GHZ states, alongside spin-squeezed states, are typically considered. Different from spin-squeezed states, where the enhancement originates from the lower shot noise, GHZ states improve the sensitivity as the phase of a collective N -qubit state evolves N times faster

compared to a single qubit state [17]. In the absence of noise, GHZ states are optimal and achieve Heisenberg scaling [8]. Moreover, they were used in Refs. [18] and [19] to demonstrate an enhanced uncertainty scaling in the presence of non-Markovian dephasing noise that is uncorrelated between subsequent experiments. In this section, we repeat the derivation from Sec. III using GHZ states as input. For simplicity, we restrict the derivation of the estimation uncertainty and its analysis to spatially uncorrelated noise.

The protocol for Ramsey spectroscopy with GHZ states consists of the following steps:

1. Preparation of an N -qubit GHZ state $|\text{GHZ}\rangle = \frac{1}{\sqrt{2}} (|0\rangle^{\otimes N} + |1\rangle^{\otimes N})$;
2. Free evolution of the system for a time τ ;
3. Projection measurement onto the initial GHZ state;
4. Repetition of steps 1-3 for $L = T/\tau$ iterations.

Unlike the protocols for separable input states and spin-squeezed input states, this protocol does not involve Ramsey pulses. The parameters of the protocol to optimize are the operating point $b_r\tau$ and the interrogation time τ .

Given the combined state of all L experimental runs and N qubits, we define the measurement operator for the l -th experiment that operates on this total state as

$$M_l(0) = 2 \left(\bigotimes_{i=1}^{l-1} \mathbb{I}_i \otimes |\text{GHZ}\rangle_l \langle \text{GHZ}| \otimes \bigotimes_{i=l+1}^L \mathbb{I}_i \right) - \mathbb{I}^{\otimes L}, \quad (\text{D1})$$

where we have rescaled the measurement operator such that the measurement outcomes are in $[-1, 1]$. Following the derivation in Sec. III, we find $M_l(\tau)$ in the Heisenberg picture with the effective Hamiltonian of Eq. (3) for a fixed interrogation time τ . The evolution of the parts proportional to the identity is trivial. The GHZ state $|\text{GHZ}\rangle_l$ in the projection operator evolves as:

$$\begin{aligned} |\text{GHZ}(\tau)\rangle_l &= \frac{1}{\sqrt{2}} \left[|0\rangle^{\otimes N} + e^{i\Sigma_n(b_r\tau + \phi_{nl\tau})} |1\rangle^{\otimes N} \right] \\ &= \frac{1}{\sqrt{2}} \left[|0\rangle^{\otimes N} + e^{i(\theta + \Sigma_n \phi_{nl\tau})} |1\rangle^{\otimes N} \right], \end{aligned} \quad (\text{D2})$$

where we have introduced the phase $\theta = Nb_r\tau$. The expectation value of the l -th measurement is obtained by computing the inner product between the evolved GHZ state and the initial GHZ state, followed by averaging over noise trajectories. Assuming spatially uncorrelated, Gaussian distributed noise, we find

$$\langle M_l(\tau) \rangle = e^{-\frac{N\gamma(\tau)}{2}} \cos(\theta). \quad (\text{D3})$$

The response of the measurement to signal changes is given by

$$\left| \frac{\partial \langle M_l(\tau) \rangle}{\partial \theta} \frac{\partial \theta}{\partial b} \right| = N\tau e^{-\frac{N\gamma(\tau)}{2}} |\sin(\theta)|, \quad (\text{D4})$$

which reaches its maximum at $\theta = q\pi/2$ for odd integers q . Choosing this value as the operating point of the sensor, we can evaluate the estimation uncertainty,

$$\Delta b_{\text{est}} = \frac{\Delta [\sum_l M_l(\tau)]}{L \left| \frac{\partial \langle M_0(\tau) \rangle}{\partial b} \right|}. \quad (\text{D5})$$

Applying the same identities introduced in Sec. III, we arrive at the following expression for the estimation uncertainty in Ramsey spectroscopy with GHZ states:

$$(\Delta b_{\text{est}})^2 = \frac{Le^{N\gamma(\tau)} + \sum_{l \neq l'} \sinh(N \langle \phi_{l0\tau} \phi_{l'0\tau} \rangle)}{N^2 T^2}. \quad (\text{D6})$$

For easier interpretation, we can simplify this expression by using the first-order sinh approximation as in Sec. IV C. With this, we arrive at

$$(\Delta b_{\text{est}})^2 = \frac{Le^{N\gamma(\tau)} - NL\gamma(\tau) + N\gamma(T)}{N^2 T^2}. \quad (\text{D7})$$

In the absence of noise, we recover the Heisenberg scaling $\Delta b_{\text{est}} = 1/(N\sqrt{T\tau})$ [8]. For Markovian noise $\gamma(\tau) = A\tau$, the optimal interrogation time is $\tau = 1/(NA)$, leading to an uncertainty of $\Delta b_{\text{est}} = \sqrt{Ae}/\sqrt{NT}$. This matches the estimation uncertainty obtained with separable input states [11], resulting in no metrological gain $r = 1$ independent of N .

Fig. 8 shows the result of estimation using GHZ states. It is the equivalent of Fig. 3 but for GHZ- instead of spin-squeezed states. In Fig. 8a, the minimal normalized uncertainty is plotted against the number of qubits. We observe the above-discussed absence of an advantage of GHZ-states over separable states in the case of white noise, leading to $r = 1$ in Fig. 8b.

For noise with Gaussian and Ohmic spectrum, where $\gamma(\tau) \propto \tau^2$ at short interrogation times τ , the optimal interrogation time scales as $\tau_{\text{opt}} \propto 1/\sqrt{N}$, see Fig. 8c. The estimation uncertainty scaling for Gaussian and Ohmic spectra is very similar to that obtained with spin-squeezed states. In particular, as visible in Fig. 8b, a scaling of $\Delta b_{\text{est}} \propto N^{-3/4}$ is achieved for Ohmic noise, while Gaussian noise results in $\Delta b_{\text{est}} \propto 1/\sqrt{N}$, as the fundamental limit of Eq. (6) still applies.

A difference in the scaling of the estimation uncertainty between GHZ states and spin-squeezed states appears for noise with a linear spectrum. While spin-squeezed input states offer a scaling advantage over separable states, GHZ states perform worse than separable input states. For the linear spectrum [see Eq. (24)] the dephasing $\gamma(\tau)$ can in the regime $\sigma\tau < 1$ be approximated as $\gamma(\tau) \approx A\tau(1 - \frac{\tau\sigma}{\pi})$. When $\sigma\tau/\pi < 1$, the linear behavior dominates, and we write $\gamma(\tau) \approx \tilde{A}\tau$, where the noise strength \tilde{A} is weakly time dependent. This leads to an estimation uncertainty $\Delta b_{\text{est}} = [\tilde{A}(e-1)/(NT)]^{1/2}$ for both GHZ and separable input states. However, while for GHZ states \tilde{A} approaches A for large N , \tilde{A} is smaller for separable states due to the longer optimal interrogation

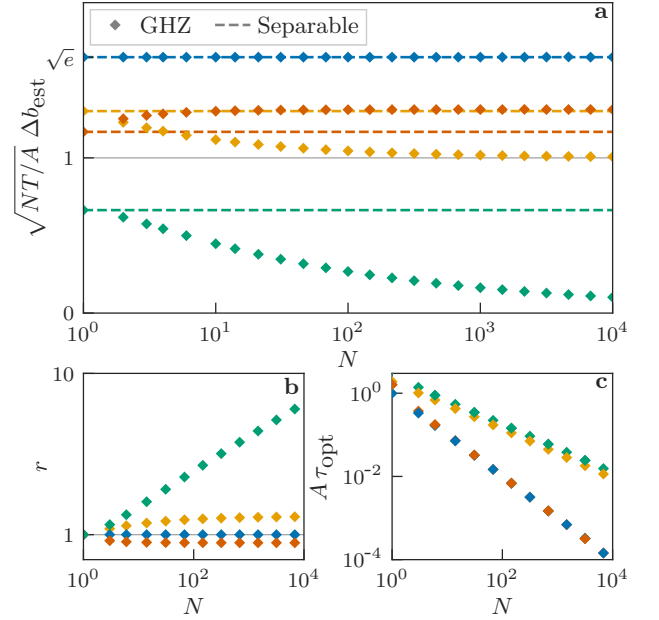


Figure 8. Estimation uncertainty in Ramsey spectroscopy with GHZ input states under various noise spectra (plotted in Fig. 3a), for a certain total probing time T much larger than the noise correlation time and dephasing time. (a) Scaled uncertainty $\sqrt{NT/A} \Delta b_{\text{est}}$ as a function of the number of qubits N for GHZ input states compared to separable input states with (counting from below at $N = 1$) Ohmic, linear, Gaussian, and white spectra. (b) Metrological gain r of estimation uncertainties between separable and GHZ input states as a function of N . (c) Optimal interrogation time τ_{opt} for GHZ input states versus N .

time. Consequently, separable states achieve a lower estimation uncertainty than GHZ states, as shown in Fig. 8.

Spin-squeezed states have the advantage that the amount of entanglement is tunable. This freedom allows one to achieve better performance with spin-squeezed states than with separable or maximally entangled states. A similar advantage could perhaps be gained with GHZ states by preparing a state $|\Phi\rangle$ consisting of N/S GHZ states of size S ,

$$|\Phi\rangle = \bigotimes_{i=1}^{N/S} \frac{1}{\sqrt{2}} \left(|0\rangle^{\otimes S} + |1\rangle^{\otimes S} \right). \quad (\text{D8})$$

For spatially uncorrelated noise, the measurement outcomes for each of the N/S blocks are uncorrelated. For fixed size S , this leads to a total estimation uncertainty scaling proportional to $1/\sqrt{N}$, due to the statistical averaging over N/S independent estimates. Hence, for spatially uncorrelated noise, this strategy does not provide a scaling advantage over separable input states. However, the situation may change when the noise is spatially correlated, opening up many different strategies to exploit the spatial structure. A detailed discussion of this possibility is, however, beyond the scope of this work.

-
- [1] K. A. Gilmore, M. Affolter, R. J. Lewis-Swan, D. Barberena, E. Jordan, A. M. Rey, and J. J. Bollinger, Quantum-enhanced sensing of displacements and electric fields with two-dimensional trapped-ion crystals, *Science* **373**, 673 (2021).
- [2] J. Ye and P. Zoller, Essay: Quantum sensing with atomic, molecular, and optical platforms for fundamental physics, *Phys. Rev. Lett.* **132**, 190001 (2024).
- [3] C. M. Caves, Quantum-mechanical noise in an interferometer, *Phys. Rev. D* **23**, 1693 (1981).
- [4] M. Tse, et al., and LIGO Scientific Collaboration, Quantum-enhanced advanced ligo detectors in the era of gravitational-wave astronomy, *Phys. Rev. Lett.* **123**, 231107 (2019).
- [5] F. Acernese, et al., and Virgo Collaboration, Increasing the astrophysical reach of the advanced virgo detector via the application of squeezed vacuum states of light, *Phys. Rev. Lett.* **123**, 231108 (2019).
- [6] V. Giovannetti, S. Lloyd, and L. Maccone, Quantum metrology, *Phys. Rev. Lett.* **96**, 010401 (2006).
- [7] V. Giovannetti, S. Lloyd, and L. Maccone, Quantum-enhanced measurements: Beating the standard quantum limit, *Science* **306**, 1330 (2004).
- [8] J. J. . Bollinger, W. M. Itano, D. J. Wineland, and D. J. Heinzen, Optimal frequency measurements with maximally correlated states, *Phys. Rev. A* **54**, R4649 (1996).
- [9] Z. Y. Ou, Fundamental quantum limit in precision phase measurement, *Phys. Rev. A* **55**, 2598 (1997).
- [10] B. Yurke, S. L. McCall, and J. R. Klauder, $Su(2)$ and $su(1,1)$ interferometers, *Phys. Rev. A* **33**, 4033 (1986).
- [11] S. F. Huelga, C. Macchiavello, T. Pellizzari, A. K. Ekert, M. B. Plenio, and J. I. Cirac, Improvement of frequency standards with quantum entanglement, *Phys. Rev. Lett.* **79**, 3865 (1997).
- [12] B. Escher, R. L. de Matos Filho, and L. Davidovich, General framework for estimating the ultimate precision limit in noisy quantum-enhanced metrology, *Nature Physics* **7**, 406 (2011).
- [13] C. L. Degen, F. Reinhard, and P. Cappellaro, Quantum sensing, *Rev. Mod. Phys.* **89**, 035002 (2017).
- [14] J. F. Haase, A. Smirne, S. Huelga, J. Kolodynski, and R. Demkowicz-Dobrzanski, Precision limits in quantum metrology with open quantum systems, *Quantum Measurements and Quantum Metrology* **5**, 13 (2016).
- [15] D. J. Wineland, J. J. Bollinger, W. M. Itano, F. L. Moore, and D. J. Heinzen, Spin squeezing and reduced quantum noise in spectroscopy, *Phys. Rev. A* **46**, R6797 (1992).
- [16] D. J. Wineland, J. J. Bollinger, W. M. Itano, and D. J. Heinzen, Squeezed atomic states and projection noise in spectroscopy, *Phys. Rev. A* **50**, 67 (1994).
- [17] D. Ulam-Orgikh and M. Kitagawa, Spin squeezing and decoherence limit in ramsey spectroscopy, *Phys. Rev. A* **64**, 052106 (2001).
- [18] Y. Matsuzaki, S. C. Benjamin, and J. Fitzsimons, Magnetic field sensing beyond the standard quantum limit under the effect of decoherence, *Phys. Rev. A* **84**, 012103 (2011).
- [19] A. W. Chin, S. F. Huelga, and M. B. Plenio, Quantum metrology in non-markovian environments, *Phys. Rev. Lett.* **109**, 233601 (2012).
- [20] K. Macieszczak, Zeno limit in frequency estimation with non-markovian environments, *Phys. Rev. A* **92**, 010102 (2015).
- [21] A. Smirne, J. Kołodyński, S. F. Huelga, and R. Demkowicz-Dobrzański, Ultimate precision limits for noisy frequency estimation, *Phys. Rev. Lett.* **116**, 120801 (2016).
- [22] J. F. Haase, A. Smirne, J. Kołodyński, R. Demkowicz-Dobrzański, and S. F. Huelga, Fundamental limits to frequency estimation: a comprehensive microscopic perspective, *New Journal of Physics* **20**, 053009 (2018).
- [23] S. L. Braunstein and C. M. Caves, Statistical distance and the geometry of quantum states, *Phys. Rev. Lett.* **72**, 3439 (1994).
- [24] Y. Yang, V. Montenegro, and A. Bayat, Extractable information capacity in sequential measurements metrology, *Phys. Rev. Res.* **5**, 043273 (2023).
- [25] E. O'Connor, S. Campbell, and G. T. Landi, Fisher information rates in sequentially measured quantum systems, *New Journal of Physics* **26**, 033048 (2024).
- [26] C. F. Ockeloen, R. Schmied, M. F. Riedel, and P. Treutlein, Quantum metrology with a scanning probe atom interferometer, *Phys. Rev. Lett.* **111**, 143001 (2013).
- [27] U. Dorner, Quantum frequency estimation with trapped ions and atoms, *New Journal of Physics* **14**, 043011 (2012).
- [28] F. Beaudoin, L. M. Norris, and L. Viola, Ramsey interferometry in correlated quantum noise environments, *Phys. Rev. A* **98**, 020102 (2018).
- [29] F. Riberi and L. Viola, Optimal asymptotic precision bounds for nonlinear quantum metrology under collective dephasing, *APL Quantum* **2**, 026111 (2025).
- [30] F. Riberi, L. M. Norris, F. Beaudoin, and L. Viola, Frequency estimation under non-markovian spatially correlated quantum noise, *New Journal of Physics* **24**, 103011 (2022).
- [31] F. Riberi, G. A. Paz-Silva, and L. Viola, Nearly heisenberg-limited noise-unbiased frequency estimation by tailored sensor design, *Phys. Rev. A* **108**, 042419 (2023).
- [32] A. J. Brady, Y.-X. Wang, V. V. Albert, A. V. Gorshkov, and Q. Zhuang, Correlated noise estimation with quantum sensor networks, *Phys. Rev. Lett.* **136**, 080803 (2026).
- [33] E. M. Kessler, P. Kómár, M. Bishof, L. Jiang, A. S. Sørensen, J. Ye, and M. D. Lukin, Heisenberg-limited atom clocks based on entangled qubits, *Phys. Rev. Lett.* **112**, 190403 (2014).
- [34] L. Pezzè and A. Smerzi, Heisenberg-limited noisy atomic clock using a hybrid coherent and squeezed state protocol, *Phys. Rev. Lett.* **125**, 210503 (2020).
- [35] T. Kielinski and K. Hammerer, Bayesian frequency metrology with optimal ramsey interferometry in optical atomic clocks, *Reports on Progress in Physics* **88**, 124001 (2025).
- [36] R. Chaves, J. B. Brask, M. Markiewicz, J. Kołodyński, and A. Acín, Noisy metrology beyond the standard quantum limit, *Phys. Rev. Lett.* **111**, 120401 (2013).
- [37] A. A. Clerk, M. H. Devoret, S. M. Girvin, F. Marquardt, and R. J. Schoelkopf, Introduction to quantum noise, measurement, and amplification, *Rev. Mod. Phys.* **82**, 1155 (2010).

- [38] P. Szańkowski, M. Trippenbach, and J. Chwedeńczuk, Parameter estimation in memory-assisted noisy quantum interferometry, *Phys. Rev. A* **90**, 063619 (2014).
- [39] B. Gu and I. Franco, When can quantum decoherence be mimicked by classical noise?, *The Journal of Chemical Physics* **151**, 014109 (2019).
- [40] R. Demkowicz-Dobrzański, J. Kołodyński, and M. Guţă, The elusive heisenberg limit in quantum-enhanced metrology, *Nature communications* **3**, 1063 (2012).
- [41] S. Seah, S. Nimmrichter, D. Grimmer, J. P. Santos, V. Scarani, and G. T. Landi, Collisional quantum thermometry, *Phys. Rev. Lett.* **123**, 180602 (2019).
- [42] Y. Yang, V. Montenegro, and A. Bayat, Sequential-measurement thermometry with quantum many-body probes, *Phys. Rev. Appl.* **22**, 024069 (2024).
- [43] M. Kitagawa and M. Ueda, Squeezed spin states, *Phys. Rev. A* **47**, 5138 (1993).
- [44] J. Borregaard and A. S. Sørensen, Near-heisenberg-limited atomic clocks in the presence of decoherence, *Phys. Rev. Lett.* **111**, 090801 (2013).
- [45] L. Pezzè, A. Smerzi, M. K. Oberthaler, R. Schmied, and P. Treutlein, Quantum metrology with nonclassical states of atomic ensembles, *Rev. Mod. Phys.* **90**, 035005 (2018).
- [46] W. M. Itano, J. C. Bergquist, J. J. Bollinger, J. M. Gilligan, D. J. Heinzen, F. L. Moore, M. G. Raizen, and D. J. Wineland, Quantum projection noise: Population fluctuations in two-level systems, *Phys. Rev. A* **47**, 3554 (1993).
- [47] J. Ma, X. Wang, C. Sun, and F. Nori, Quantum spin squeezing, *Physics Reports* **509**, 89 (2011).
- [48] G. S. Uhrig, Exact results on dynamical decoupling by π pulses in quantum information processes, *New Journal of Physics* **10**, 083024 (2008).
- [49] M. J. Biercuk, A. C. Doherty, and H. Uys, Dynamical decoupling sequence construction as a filter-design problem, *Journal of Physics B: Atomic, Molecular and Optical Physics* **44**, 154002 (2011).
- [50] R. E. Ziemer and W. H. Tranter, *Principles of communications* (John Wiley & Sons, 2014).
- [51] C. Luo, H. Zhang, A. Chu, C. Maruko, A. M. Rey, and J. K. Thompson, Hamiltonian engineering of collective xyz spin models in an optical cavity, *Nature Physics* , 1 (2025).